

RESEARCH LETTER

10.1029/2018GL078719

Key Points:

- Mechanisms of ocean heat transport into the Arctic, that is, across 70°N, are distinct under internal variability and climate change
- Under decadal internal variability, increased northward heat transport at 70°N is linked to strong midlatitude meridional overturning
- Under greenhouse gas forcing, midlatitude overturning weakens, yet northward heat transport at 70°N increases due to regional circulations

Supporting Information:

- Supporting Information S1

Correspondence to:

D. Oldenburg,
oldend@uw.edu

Citation:

Oldenburg, D., Armour, K. C., Thompson, L., & Bitz, C. (2018). Distinct mechanisms of ocean heat transport into the Arctic under internal variability and climate change. *Geophysical Research Letters*, 45. <https://doi.org/10.1029/2018GL078719>

Received 10 MAY 2018

Accepted 16 JUL 2018

Accepted article online 25 JUL 2018

Distinct Mechanisms of Ocean Heat Transport Into the Arctic Under Internal Variability and Climate Change

Dylan Oldenburg¹ , Kyle C. Armour^{1,2} , LuAnne Thompson¹ , and Cecilia M. Bitz² 

¹School of Oceanography, University of Washington, Seattle, WA, USA, ²Department of Atmospheric Sciences, University of Washington, Seattle, WA, USA

Abstract Northward ocean heat transport (OHT) plays a key role in Arctic climate variability and change. Unforced climate model simulations suggest that at decadal and longer timescales, strengthened Atlantic meridional overturning circulation (AMOC) is correlated with increased OHT into the Arctic. Yet greenhouse gas forced simulations predict increased Arctic OHT while AMOC weakens. Here we partition OHT changes into contributions from *dynamic* circulation changes and *thermodynamic* temperature advection, as well as meridional overturning and gyre changes. We find that under decadal-scale internal variability, strengthened AMOC converges heat in the subpolar gyre; anomalous heat is advected into the Arctic by both time mean circulations and strengthened gyre circulations. Under greenhouse gas forcing, weakened AMOC reduces subpolar gyre heat convergence; yet Arctic OHT increases as mean overturning and strengthened gyre circulations advect warmed surface waters. Thus, caution should be exercised when inferring Arctic OHT from AMOC, as the relationship between OHT and AMOC changes depends on whether they are internally generated or externally forced.

Plain Language Summary Relatively warm currents flow northward from the Atlantic into the Arctic Ocean, acting to warm Arctic climate. Changes in the strength or temperature of these currents are thought to play an important role in Arctic climate change and variability. Using climate models, we show that natural fluctuations in heat transport into the Arctic are linked to changes in currents further south. In particular, when the Atlantic meridional overturning circulation (AMOC) is strong, warmer waters are delivered to the subpolar gyre near Greenland and subsequently carried northward. AMOC is expected to weaken under greenhouse gas (GHG) forcing, suggesting that heat transport into the Arctic may decrease if the same mechanisms apply to climate change. However, climate models predict increased heat transport into the Arctic under GHG forcing, even while AMOC slows, enhancing Arctic warming. This occurs because GHGs (i) warm surface waters, increasing the heat carried by northward-flowing currents and (ii) change ocean currents near Greenland, increasing the flow of already warm waters. Our results indicate that different mechanisms govern changes in ocean heat transport into the Arctic under variability and GHG warming. Thus, caution should be taken when predicting how Arctic climate will be affected by AMOC changes over coming decades.

1. Introduction

The Arctic has been warming more than twice as rapidly as global average temperature over recent decades (Marshall et al., 2014; Serreze et al., 2009). This Arctic amplification of greenhouse gas (GHG) warming is also a robust feature of global climate model simulations (e.g., Holland & Bitz, 2003; Marshall et al., 2015, 2014; Pithan & Mauritsen, 2014). There is growing evidence that variations in northward ocean heat transport (OHT) into the Arctic from the North Atlantic Ocean play a key role in driving changes in Arctic climate under both internal variability and GHG-induced warming.

Recent studies suggest that the strength of the Atlantic meridional overturning circulation (AMOC) influences Arctic temperature and sea ice extent on decadal and longer timescales (Chylek et al., 2014; Day et al., 2012; Delworth et al., 2016; Li et al., 2017; Mahajan et al., 2011; Yeager et al., 2015; Zhang, 2015). The apparent mechanism is that strong AMOC leads to enhanced OHT throughout the North Atlantic extending into the higher latitudes through the transport of warmer Atlantic water through the Barents Sea and Eastern Fram Strait (Delworth et al., 2016; Li et al., 2017; Yeager et al., 2015; Zhang, 2015). This suggests a link between variations

in AMOC and OHT into the Arctic, with AMOC and associated subpolar gyre (SPG) changes perhaps driven by variability in buoyancy forcing associated with the North Atlantic Oscillation (NAO; Delworth et al., 2016; Delworth & Zeng, 2016; Yeager et al., 2015). Indeed, it has been proposed that a period of strengthened AMOC in recent decades has contributed to the observed high rate of Arctic warming and sea ice loss (Chylek et al., 2014; Delworth et al., 2016; Li et al., 2017; Yeager et al., 2015; Zhang, 2015), which is supported by observations showing increased OHT into the Arctic in the Atlantic sector (Dmitrenko et al., 2008; Schauer et al., 2004; Skagseth et al., 2008).

Do similar mechanisms arise under GHG-induced warming? Climate models robustly predict weakening AMOC under GHG forcing, in turn reducing northward heat transport into the SPG (Gregory et al., 2005; Huber & Zanna, 2017; Jungclaus et al., 2014; Kostov et al., 2014; Marshall et al., 2015; Nummelin et al., 2017; Rugenstein et al., 2013). Based on the connection between AMOC and OHT seen under internal variability, weakened AMOC should lead to decreased OHT into the Arctic, reducing the pace of Arctic warming and sea ice loss. Indeed, slower sea ice loss has been predicted for the next decade based on modeled AMOC declines (Mahajan et al., 2011; Yeager et al., 2015). However, models robustly predict an *increase* in OHT into the Arctic while AMOC weakens under GHG forcing (Bitz et al., 2006; Holland & Bitz, 2003; Hwang et al., 2011; Jungclaus et al., 2014; Koenig & Brodeau, 2014; Mahlstein & Knutti, 2011; Marshall et al., 2015; Nummelin et al., 2017; Rugenstein et al., 2013)—at odds with expectations based on internal variability. Moreover, increased OHT into the Arctic (e.g., across 70°N) is correlated with the degree of Arctic amplification simulated across models, with increased OHT associated with greater Arctic warming and sea ice loss (Mahlstein & Knutti, 2011; Nummelin et al., 2017; Holland & Bitz, 2003; Hwang et al., 2011).

Accurate predictions of future Arctic climate and sea ice thus hinge on our ability to predict how OHT will evolve in the future. A key question is, will the recent AMOC weakening (e.g., Caesar et al., 2018; Smeed et al., 2014; Thornalley et al., 2018) result in increased or decreased OHT into the Arctic? Answering this question requires a mechanistic understanding of how the links between AMOC, the SPG circulation, and OHT into the Arctic differ under internal variability and GHG forcing.

Different patterns of Atlantic OHT under internal variability and GHG forcing are a robust feature of comprehensive global climate models, such as those participating in phase 5 of the Coupled Model Intercomparison Project (CMIP5; Taylor et al., 2012). In unforced preindustrial (PI) control simulations, decadal variations in OHT into the Arctic (taken at 70°N here, henceforth referred to as OHT_{70}) occur with a strong meridional coherence. That is, OHT anomalies (OHT') have the same sign throughout the North Atlantic basin, from the tropics to the pole (Figure 1a). During decades when OHT_{70} is anomalously large, heat is anomalously converged in the SPG and Arctic, while during decades when OHT_{70} is anomalously weak, heat is anomalously diverged from the SPG and Arctic. In contrast, under GHG forcing (abrupt CO_2 quadrupling shown here), OHT_{70} increases even while OHT decreases throughout the middle to low latitudes (Figure 1b), concurrent with AMOC weakening (Gregory et al., 2005; Kostov et al., 2014). These OHT anomalies under GHG forcing result in (i) anomalous divergence of heat, and thus cooling or reduced warming, within the SPG (Marshall et al., 2015; Menary et al., 2015; Singh et al., 2017) and (ii) anomalous convergence of heat at higher latitudes, enhancing Arctic warming (Marshall et al., 2015; Nummelin et al., 2017; Singh et al., 2017).

Here we focus on mechanisms of Atlantic OHT changes in one particular model, the Community Climate System Model Version 4 (CCSM4; Gent et al., 2011), that simulates changes consistent with the behavior seen across CMIP5 models (Figure 1). We seek to develop a mechanistic understanding of how changes in AMOC and SPG circulation are connected to OHT further north within the Nordic Seas and of how the operation of these mechanisms may differ under GHG forcing and internal variability. In particular, we decompose and interpret OHT changes at different latitudes in terms of *dynamic* changes in ocean circulation versus *thermodynamic* temperature advection and in terms of meridional overturning and gyre circulations. Following recent papers on the topic (e.g., Koenig & Brodeau, 2014; Zhang, 2015), we focus on northward OHT crossing the Arctic Circle (taken here to be around 70°N), which is representative of OHT into the high latitudes.

2. Methods

To examine the mechanisms of OHT changes under internal variability, we use CCSM4's PI control simulation, which is 1,300 years long and unforced (with constant 1850s GHG and aerosol levels and no volcanic eruptions). For GHG forcing, we consider CCSM4's 150-year-long simulation of abrupt CO_2 quadrupling ($4 \times CO_2$) relative to PI levels. We remove linear drifts over the PI control from all variables prior to analysis. The $4 \times CO_2$

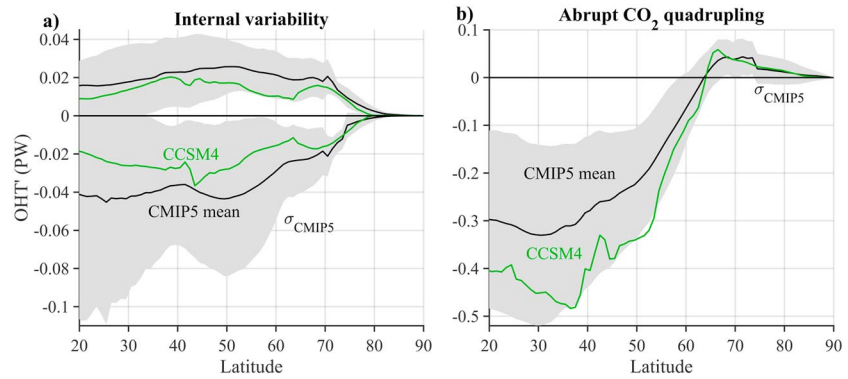


Figure 1. OHT' under internal variability and abrupt CO₂ quadrupling simulations of CMIP5 models. (a) OHT' during decades of preindustrial control simulations in which OHT'₇₀ is greater than 1.5σ (top curves) and less than −1.5σ (bottom curves) relative to its long-term average. (b) OHT' (relative to the preindustrial) at year 100 following abrupt CO₂ quadrupling. The black curves show CMIP5 mean (see supporting information Figure S4 for the list of models), the gray shading shows the standard deviation across CMIP5 models, and the green curves show CCSM4. OHT' values are computed from model output OHT (“hfbasin” in the CMIP5 archive) for all CMIP5 models except CCSM4, for which we compute OHT' from the velocity and temperature fields (section 2). CCSM4 = Community Climate System Model Version 4; CMIP5 = Coupled Model Intercomparison Project; OHT = ocean heat transport.

simulation allows us to study the ocean’s time-dependent response to CO₂ forcing without having to account for the temporal variations of GHGs or other forcing agents and is a sufficiently large forcing that changes are well outside the bounds of internal variability. Our analysis of forced response thus differs from previous studies that consider OHT changes under specific historical and future emissions scenarios (Bitz et al., 2006; Jungclaus et al., 2014; Nummelin et al., 2017). We focus on OHT into the Arctic from the Atlantic sector since it is substantially larger than OHT in the Pacific sector (across Bering Strait) in both time mean and anomalies under internal variability and GHG forcing.

2.1. Calculating OHT and Its Components

OHT as a function of latitude and time is given by

$$\text{OHT}(y, t) = \rho c_p \int_{x_1}^{x_2} \int_{z_{\text{bot}}}^0 v \theta dz dx, \quad (1)$$

where ρ is the density, which is assumed to be uniform, and c_p is the heat capacity of seawater; z_{bot} is the ocean bottom depth; x_1 and x_2 are the longitude limits; θ is the monthly potential temperature as a function of x (longitude), y (latitude), z (depth), and t (time); and v is the monthly resolved Eulerian mean velocity. Bolus, diffusion, and submesoscale flux terms make negligible contributions to OHT or its changes within the domain of our analysis (North Atlantic and Nordic Seas). Errors in OHT introduced by using monthly mean velocity and temperature are estimated to be of order a few percent at all latitudes.

Borrowing the terminology of previous studies (e.g., Bony et al., 2004), OHT anomalies can be decomposed into contributions from (i) dynamic changes in circulation (anomalous currents advecting time mean heat content), (ii) thermodynamic changes in temperature (anomalous heat advected by time mean circulations), and (iii) a *nonlinear* term representing the higher-order contributions to OHT' from simultaneous changes in temperature and circulation:

$$\text{OHT}'(y, t) = \underbrace{\rho c_p \int_{x_1}^{x_2} \int_{z_{\text{bot}}}^0 \bar{v} \theta' dz dx}_{\text{thermodynamic}} + \underbrace{\rho c_p \int_{x_1}^{x_2} \int_{z_{\text{bot}}}^0 v' \bar{\theta} dz dx}_{\text{dynamic}} + \underbrace{\rho c_p \int_{x_1}^{x_2} \int_{z_{\text{bot}}}^0 v' \theta' dz dx}_{\text{nonlinear}}, \quad (2)$$

where overbars represent a time mean of a given variable (i.e., \bar{v} and $\bar{\theta}$) and primes represent temporal anomalies of a variable relative to its time mean (i.e., v' and θ').

The grid of the ocean model within CCSM4 is not rectilinear. The OHT calculation is started by a direct calculation of OHT at 34°S, the southernmost tip of Africa, where the east-west grid line follows a line of constant latitude. Then, using the model T , u , and v fields, the divergence of heat transport for each T grid cell is calculated. The OHT at each target latitude north of 34°S is then calculated as the sum of the divergence of all T grid

cells between the target latitude and 34°S plus the OHT at 34°S. We follow the same procedure for computing the dynamic, thermodynamic, and nonlinear components.

We further decompose dynamic, thermodynamic, and nonlinear OHT' into overturning and gyre components. The overturning components of each are calculated from the zonal mean potential temperature, $\langle \theta \rangle$, and the meridional overturning stream function, ψ , according to

$$\text{OHT}'_{\text{MOC}}(y, t) = \underbrace{\rho c_p \int_{z_{\text{bot}}}^0 \bar{\psi} \frac{\partial \langle \theta \rangle'}{\partial z} dz}_{\text{thermodynamic}} + \underbrace{\rho c_p \int_{z_{\text{bot}}}^0 \psi' \frac{\partial \langle \theta \rangle'}{\partial z} dz}_{\text{dynamic}} + \underbrace{\rho c_p \int_{z_{\text{bot}}}^0 \psi' \frac{\partial \langle \theta \rangle'}{\partial z} dz}_{\text{nonlinear}}, \quad (3)$$

where

$$\psi(y, z, t) = - \int_z^0 \int_{x_1}^{x_2} v(x, y, \bar{z}, t) dx d\bar{z}. \quad (4)$$

The gyre component of OHT can be expressed as

$$\text{OHT}'_{\text{gyre}}(y, t) = \rho c_p \int_{z_{\text{bot}}}^0 \int_{x_1}^{x_2} \dot{v} \dot{\theta} dx dz \quad (5)$$

where \dot{v} and $\dot{\theta}$ are anomalies relative to the zonal mean at each latitude. As is typical in observational studies (Bryden & Imawaki, 2001; Piecuch & Ponte, 2011), we calculate $\text{OHT}'_{\text{gyre}}$ as a residual between OHT' and OHT'_{MOC} . This is based on the assumptions that there is no meridional mass transport through the ocean basin and that the transport associated with parameterized eddies is small.

2.1.1. Internal Variability in OHT

Motivated by previous studies (Day et al., 2012; Delworth et al., 2016; Mahajan et al., 2011; Yeager et al., 2015; Zhang, 2015), we focus on mechanisms of internal, decadal-scale OHT variability. At decadal timescales there is a high positive correlation between OHT'_{70} and OHT' in the midlatitudes within PI control simulations (Figure 1a and supporting information Figure S1), suggesting a potential link between changes in AMOC and OHT'_{70} . This positive correlation remains high for variability at multidecadal timescales but decreases toward interannual timescales (Figure S1).

To isolate internal variability of OHT at decadal timescales, we calculate monthly Atlantic OHT over the length of CCSM4's PI control simulation and take 10-year moving averages with each interval overlapping the previous by half. For each decadal average, we calculate OHT' and its components, where anomalies are defined with respect to the time mean over the PI control. To focus on OHT into the Arctic, we conditionally average all OHT components during the 10-year periods during which OHT'_{70} is greater than 1.5 standard deviations (σ) away from its time mean value (Figure 1a); results are similar if other choices, such as 1σ or 2σ , are used instead. In the analysis below, we focus on the periods when OHT'_{70} is large for a more direct comparison to the mechanisms of increased OHT'_{70} under GHG forcing. Results are nearly symmetric for $\text{OHT}'_{70} > 1.5\sigma$ and $\text{OHT}'_{70} < -1.5\sigma$ (Figure S2).

2.1.2. GHG-Forced Changes in OHT

To analyze the mechanisms governing GHG-forced changes in OHT into the Arctic, we calculate monthly Atlantic OHT over the length of CCSM4's $4 \times \text{CO}_2$ simulation and over the concurrent 150 years of the PI control. We calculate OHT' and its components relative to the PI control. For our main analysis, we consider OHT' averaged over a 30-year period around year 100 (years 86–115) following CO_2 quadrupling; other periods, such as 30-year intervals around year 70 or year 130, yield similar results (Figure S3).

3. Results

3.1. Mechanisms of OHT Changes Under Internal Variability

During decades of the PI control simulation when $\text{OHT}'_{70} > 1.5\sigma$, OHT' is also positive from the equator to the North Pole (Figure 2a). The latitudinal variations in OHT' indicates that heat is anomalously converged over most latitudes poleward of 40°N and most strongly within the SPG (50° to 60°N) and Arctic (poleward of 70° N).

What circulations contribute to these OHT anomalies? In the midlatitudes (equatorward of about 45°N), positive OHT' arises from anomalous OHT'_{MOC} (Figure 2b), with changes in $\text{OHT}'_{\text{gyre}}$ slightly opposing the total

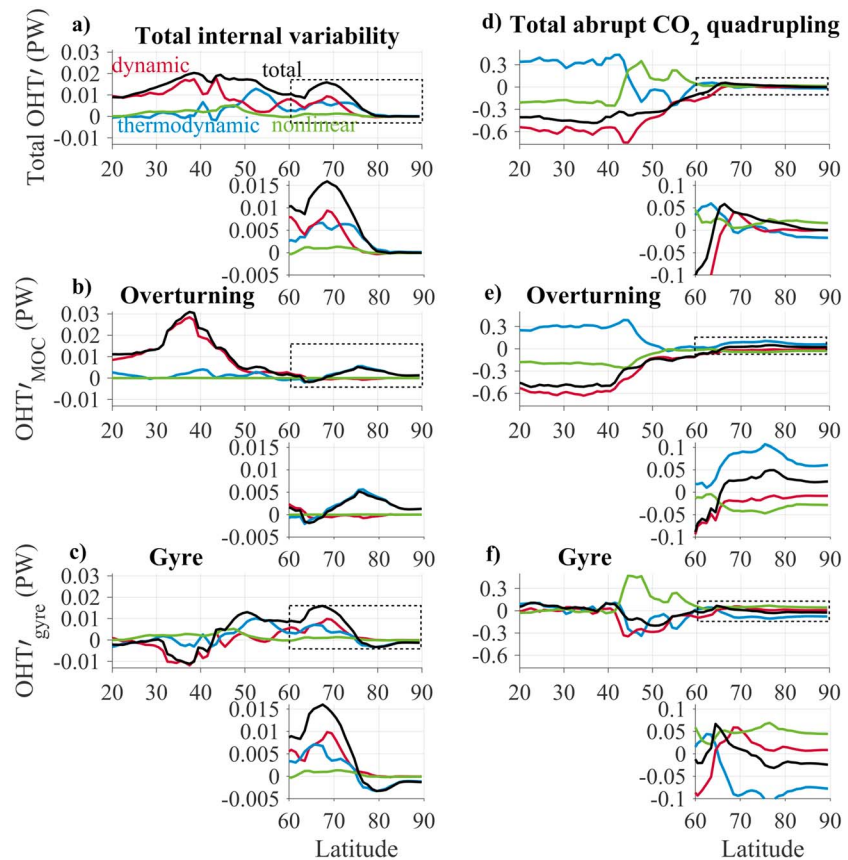


Figure 2. Overturning and gyre, as well as dynamic, thermodynamic, and nonlinear contributions to OHT' under internal variability (left) and abrupt CO_2 quadrupling (right) simulations of Community Climate System Model Version 4. (a) Total OHT' components conditionally averaged over decades in the preindustrial control simulation during which $OHT'_{70} > 1.5\sigma$. (b) Overturning OHT' components. (c) Gyre OHT' components. (d) Total OHT' components averaged over a 30-year interval centered on year 100 following an abrupt CO_2 quadrupling. (e) Overturning OHT' components. (f) Gyre OHT' components. OHT = ocean heat transport.

OHT' (Figure 2c). Moreover, midlatitude OHT' , OHT'_{MOC} , and OHT'_{gyre} primarily reflect dynamic changes in circulations, with relatively small thermodynamic and negligible nonlinear components.

Within the SPG (50° to $60^\circ N$), OHT' is positive, primarily owing to thermodynamic OHT'_{gyre} (Figure 2c). OHT' is positive in the Nordic Seas and at $70^\circ N$ primarily owing to OHT'_{gyre} , split about equally between dynamic and thermodynamic gyre changes; OHT'_{MOC} plays a minor role at these latitudes. This suggests a handoff across latitudes in which heat converged on the southern edge of the SPG by changes in meridional overturning is carried further northward by the time mean SPG circulation and converged into the Arctic by both dynamic and thermodynamic gyre circulations. Nonlinear components are, as expected, small compared to the other components since both v' and T' are small under internal variability relative to \bar{v} and \bar{T} . Values of the OHT'_{70} components under internal variability are given in Table S1.

The components of OHT' can be physically understood in terms of either time mean or anomalous circulations acting on time mean or anomalous ocean potential temperatures. Figures 3a and 3b show the MOC and potential temperature patterns conditionally averaged over the same decades during which OHT'_{70} is high. AMOC is anomalously strong during these decades (Figure 3a), consistent with positive dynamic OHT'_{MOC} in the midlatitudes. Surface waters in the midlatitudes are anomalously warm (Figure 3b), slightly enhancing the vertical temperature gradient on which the time mean overturning acts, consistent with a weak but positive thermodynamic OHT'_{MOC} in the midlatitudes. Meanwhile, the MOC weakens slightly near $70^\circ N$ (Figure 3a), but because this overturning acts on a relatively weak time mean vertical temperature gradient it has a minimal effect on OHT'_{70} . Surface waters are anomalously warm at $70^\circ N$ (Figure 3b), enhancing

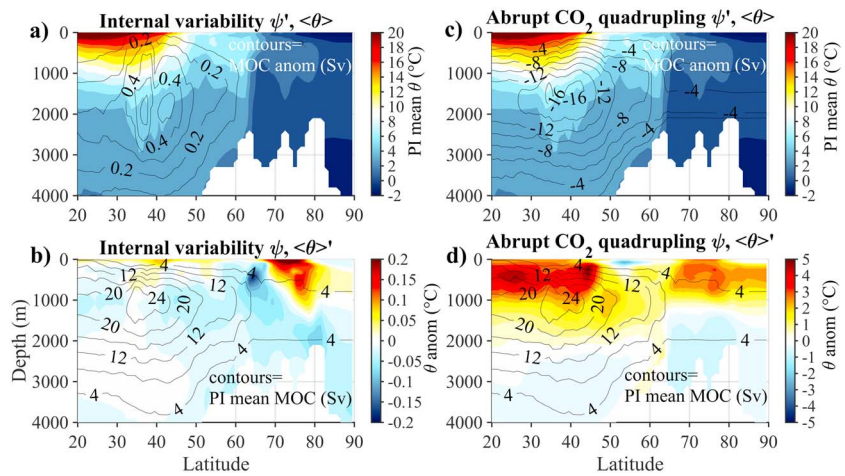


Figure 3. Meridional overturning and zonal-mean potential temperature anomalies under internal variability (left) and abrupt CO₂ quadrupling (right) simulations of CCSM4. a) MOC anomalies conditionally averaged over decades in the preindustrial simulation during which $OHT'_{70} > 1.5\sigma$ (contours, spaced every 0.1 Sv). Colors show PI control average zonal-mean θ . b) PI control average MOC (contours, spaced every 4 Sv). Colors show zonal-mean θ anomalies. c) MOC anomalies under abrupt CO₂ quadrupling (contours, spaced every 2 Sv). Colors show PI control average zonal-mean θ . d) PI control average MOC (contours, spaced every 4 Sv). Colors show zonal-mean θ anomalies.

the vertical temperature gradient on which the time mean overturning acts, consistent with a dynamic OHT'_{MOC} that contributes to OHT'_{70} .

We also consider changes associated with the barotropic circulation (Figures 4a and 4b). Because the barotropic circulation is a depth-integrated stream function, it lacks a baroclinic component and thus its heat transport only approximates OHT_{gyre} (Figure S5). Nonetheless, it is useful for gaining physical understanding. During decades when OHT'_{70} is high, the barotropic circulation is anomalously strong everywhere poleward

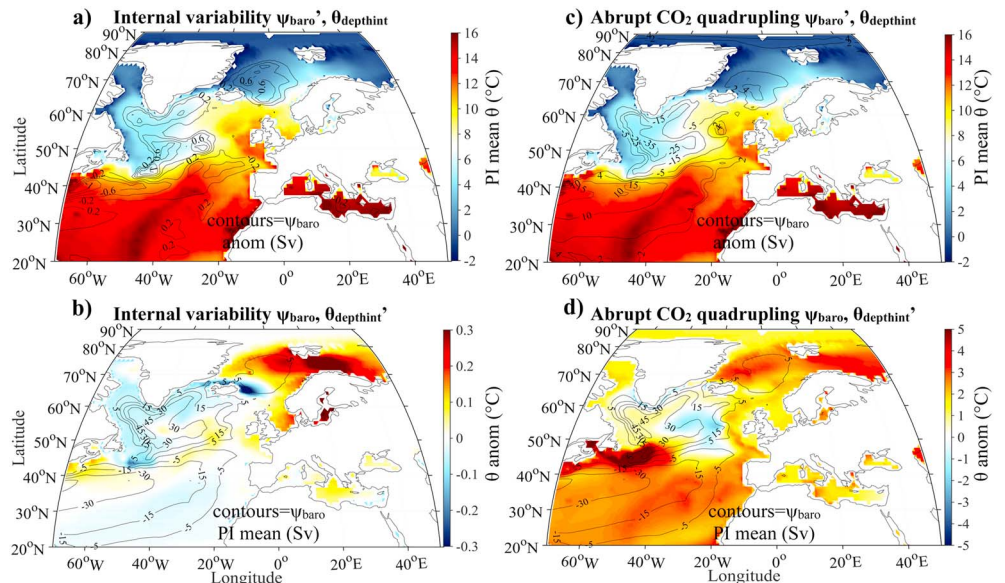


Figure 4. Barotropic stream function and depth-averaged potential temperature anomalies under internal variability (left) and abrupt CO₂ quadrupling (right) simulations of Community Climate System Model Version 4. Positive values indicate anticlockwise circulation; negative values indicate clockwise circulation. (a) Barotropic stream function anomalies conditionally averaged over decades in the preindustrial simulation during which $OHT'_{70} > 1.5\sigma$ (contours, spaced every 0.2 Sv). Colors show PI control average depth-averaged θ . (b) PI control average barotropic stream function (contours). Colors show depth-averaged θ anomalies. (c) Barotropic stream function anomalies under abrupt CO₂ quadrupling (contours). Colors show PI control average depth-averaged θ . (d) PI control average barotropic stream function (contours). Colors show depth-averaged θ anomalies. PI = preindustrial.

of about 45°N. Given that the time mean depth-averaged ocean potential temperature is generally warmer in the east than the west at these latitudes, these circulation changes are consistent with positive dynamic OHT'_{gyre} . Moreover, depth-averaged ocean potential temperature increases by more in the east than the west poleward of about 45°N, enhancing the zonal temperature gradient on which the barotropic circulation acts, consistent with positive thermodynamic OHT'_{gyre} in the SPG and at 70° N.

The results described above hold for internal variability at multidecadal (e.g., 30 years) timescales. However, at interannual timescales, OHT'_{70} variability is dominated by local gyre circulation changes at 70°N, with little changes in ocean temperature, only localized midlatitude MOC changes, and a lack of meridional coherence in OHT' (not shown). Our interpretation is that the links between OHT'_{70} and AMOC changes hold at decadal and longer timescales, while at shorter timescales OHT'_{70} changes become primarily driven by local wind variability.

3.2. Mechanisms of OHT Changes Under GHG Forcing

Averaged around year 100 following abrupt CO₂ quadrupling, OHT' is negative south of 65° and positive north of there. The variations in OHT' with latitude indicate that heat is anomalously diverged between 38°N and 42°N, anomalously converged between 42°N and 45°N, anomalously diverged between 45°N and 67°N (i.e., in the SPG), and anomalously converged between 67°N and the pole (Figure 1d).

What circulations contribute to these OHT' values? In the midlatitudes, negative OHT' is owing to both negative OHT'_{MOC} (Figure 1e) and OHT'_{gyre} (Figure 1f). Both dynamic and thermodynamic changes contribute to OHT'_{MOC} and OHT'_{gyre} . For OHT'_{MOC} , the negative dynamic component is about twice the magnitude of the positive thermodynamic component, and hence, the total OHT'_{MOC} is negative.

Within the SPG (50° to 60°N), OHT' is negative owing to both dynamic and thermodynamic OHT'_{gyre} (Figure 2f), with a small contribution from dynamic OHT'_{MOC} . Positive OHT' in the Nordic Seas and at 70°N primarily reflects positive OHT'_{MOC} , split between a positive thermodynamic component and a much smaller negative dynamic component. OHT'_{gyre} actually provides a negative contribution to OHT'_{70} , since the thermodynamic component at 70°N is negative and large in magnitude, overwhelming the positive dynamic component. This suggests that water warmed by GHG forcing in the high latitudes is converged into the Arctic by both thermodynamic meridional overturning and gyre circulations. The nonlinear components are comparable in magnitude to the other components because v' and T' under GHG forcing are similar in magnitude to \bar{v} and \bar{T} . Values of the OHT'_{70} components under abrupt CO₂ quadrupling are given in Table S1.

Figures 3c and 3d show the MOC and potential temperature anomalies around year 100 after abrupt CO₂ quadrupling. A weak AMOC (Figure 3c) is consistent with a negative dynamic OHT'_{MOC} in the midlatitudes. Surface waters in the midlatitudes are anomalously warm (Figure 3d), slightly enhancing the vertical temperature gradient on which the time mean overturning acts, consistent with a positive thermodynamic OHT'_{MOC} in the midlatitudes. Meanwhile, the MOC weakens near 70°N (Figure 3c), but because this overturning acts on a relatively weak time mean vertical temperature gradient it has a small effect on OHT'_{70} . Surface waters are anomalously warm at 70°N (Figure 3d), enhancing the vertical temperature gradient on which the time mean overturning acts, consistent with a positive dynamic OHT'_{MOC} that contributes to OHT'_{70} .

Meanwhile, the barotropic circulation is anomalously weak in the SPG (between 45°N and 60°N; Figure 4c). Given that the time mean depth-averaged ocean potential temperature is generally warmer in the east than the west at these latitudes, these circulation changes are consistent with a negative dynamic OHT'_{gyre} . Moreover, depth-averaged ocean potential temperature is seen to increase everywhere besides a small warming hole in the SPG, owing to a divergence of heat from the region. The depth-averaged ocean potential temperature increases by more in the west than the east poleward of about 45°N, weakening the zonal temperature gradient on which the barotropic circulation acts, consistent with a negative thermodynamic OHT'_{gyre} in the SPG and at 70°N (Figure 4d).

4. Discussion and Conclusions

Within CCSM4's PI control simulation, we find that AMOC plays a central role in changes in OHT into the Arctic under internal variability at decadal (and longer) timescales. During decades when OHT'_{70} is high, enhanced AMOC results in anomalous heat convergence at the southern flank of the SPG; anomalous heat is carried northward to the Nordic Seas primarily by the time mean SPG circulation. Within the Nordic Seas and at 70°N, high OHT' is due in about equal parts to (i) thermodynamic advection of heat by time mean gyre

circulations and (ii) dynamic heat redistribution by strengthened gyre circulations. These results suggest there is a complex handoff of heat between overturning and gyre circulations at different latitudes under internal variability, with a strong AMOC correlated with enhanced OHT_{70} .

Within CCSM4's simulation of abrupt CO_2 quadrupling, we find that both AMOC and the SPG circulation weaken substantially, resulting in less heat convergence into the SPG. Yet owing to the GHG forcing, surface waters are warmed everywhere poleward of $60^\circ N$, resulting in thermodynamic northward advection of heat by time mean circulations and heat convergence near $70^\circ N$. At $70^\circ N$, heat is anomalously carried northward by (i) thermodynamic advection by time mean overturning circulations and (ii) dynamic heat redistribution by strengthened gyre circulations. These results suggest that OHT_{70} increases under GHG forcing, despite weakening AMOC.

Previous studies of internal variability suggest that positive OHT'_{70} arises from enhanced delivery of warm waters into the Nordic Seas by AMOC and subsequent thermodynamic advection of this heat into the Arctic (Day et al., 2012; Zhang, 2015). Nummelin et al. (2017) propose a similar mechanism for positive OHT'_{70} under GHG forcing: Anomalous heat originating from reduced heat loss in the SPG is advected northward by time mean circulations. However, our results suggest that the situation is more complicated: A portion of OHT'_{70} under both internal variability and GHG forcing can be attributed to thermodynamic advection of anomalously warm water, yet the majority of OHT'_{70} arises from changes in ocean circulation at $70^\circ N$. Moreover, we find that these circulation changes at $70^\circ N$ are different under internal variability and GHG forcing. While CMIP5 models robustly show an increased OHT'_{70} , the partitioning of dynamic/thermodynamic and MOC/gyre components appears to vary between different models (e.g., Bitz et al., 2006; Jungclaus et al., 2014; Koenigk & Brodeau, 2014; Marshall et al., 2015). It thus seems possible that mechanisms driving OHT'_{70} differ between models, perhaps due to different representations of the location of deep convection and/or of transport across the Iceland/Scotland Ridge. It is also possible that more realistic forcing scenarios that include non- CO_2 forcings (e.g., aerosols) may produce different results.

We have homed in on the mechanisms of changes in OHT into the Arctic and found interactions between overturning and gyre circulations across latitudes that are distinct between decadal-scale internal variability and the response to GHG forcing. In both cases, we find that AMOC and the SPG circulation covary, consistent with what is expected from topographic coupling (Yeager, 2015). However, it is less clear how changes in overturning and gyre circulations in the Nordic Seas are related to circulation anomalies further south. One possibility is that ocean heat content anomalies in the midlatitudes, originating from AMOC variability, propagate northward (Arthun & Eldevik, 2016) and affect circulations in the Nordic Seas via changes in stratification. It is also possible that large-scale wind and buoyancy forcing (e.g., owing to NAO variability) drives simultaneous circulation changes in the midlatitudes and the Nordic Seas. Our analysis of internal variability, based on decadal averages, does not distinguish between these scenarios. Under GHG forcing, we find a substantial role for overturning and gyre circulation changes in the Nordic Seas in driving increased OHT into the Arctic, consistent with previous studies (Bitz et al., 2006; Koenigk & Brodeau, 2014; Marshall et al., 2015). Here too it is unclear whether these changes are driven by local wind and buoyancy anomalies or whether they are a response to changes in stratification arising from anomalous heat converged from further south. These mechanisms thus merit further study.

Our findings suggest that the mechanisms of changes in OHT into the Arctic differ under internal variability and climate forcing. Importantly, the relationship between anomalies in AMOC and OHT'_{70} changes sign between these two cases. Thus, knowledge of AMOC trends alone is insufficient to infer even the sign of trends in OHT into the Arctic, as it matters whether those trends are internally generated or externally forced. Caution should thus be exercised when applying the results of studies linking anomalies in AMOC and OHT_{70} under internal variability (Chylek et al., 2014; Day et al., 2012; Delworth et al., 2016; Li et al., 2017; Zhang, 2015) to predicting how Arctic climate will change in response to anticipated AMOC weakening over the coming decades.

References

- Arthun, M., & Eldevik, T. (2016). On anomalous ocean heat transport toward the Arctic and associated climate predictability. *Journal of Climate*, 29(2), 689–704. <https://doi.org/10.1175/JCLI-D-15-0448.1>
- Bitz, C. M., Gent, P. R., Woodgate, R. A., Holland, M. M., & Lindsay, R. (2006). The influence of sea ice on ocean heat uptake in response to increasing CO_2 . *Journal of Climate*, 19(11), 2437–2450. <https://doi.org/10.1175/JCLI3756.1>

Acknowledgments

The authors are grateful for support from the National Science Foundation through grant OCE-1523641 (D. O. and K. C. A.). We thank the CMIP5 climate modeling groups for making their model output available. The CMIP5 data for this study are accessible at the Earth System Grid Federation (ESGF) Portal (<https://esgf-node.llnl.gov/search/cmip5/>).

- Bony, S., Dufresne, J. L., Le Treut, H., Morcrette, J. J., & Senior, C. (2004). On dynamic and thermodynamic components of cloud changes. *Climate Dynamics*, 22, 71–86. <https://doi.org/10.1007/s00382-003-0369-6>
- Bryden, H., & Imawaki, S. (2001). Ocean heat transport. In G. Siedler, J. Church, & J. Gould (Eds.), *Ocean Circulation and Climate: Observing and Modelling the Global Ocean* (pp. 455–474). New York: Elsevier.
- Caesar, L., Rahmstorf, S., Robinson, A., Feulner, G., & Saba, V. (2018). Observed fingerprint of a weakening Atlantic Ocean overturning circulation. *Nature*, 556(7700), 191–196. <https://doi.org/10.1038/s41586-018-0006-5>
- Chylek, P., Hengartner, N., Lesins, G., Klett, J. D., Humlum, O., Wyatt, M., & Dubey, M. K. (2014). Isolating the anthropogenic component of Arctic warming. *Geophysical Research Letters*, 41(10), 3569–3576. <https://doi.org/10.1002/2014GL060184>
- Day, J. J., Hargreaves, J. C., Annan, J. D., & Abe-Ouchi, A. (2012). Sources of multi-decadal variability in Arctic sea ice extent. *Environmental Research Letters*, 7(3), 34011.
- Delworth, T. L., & Zeng, F. (2016). The impact of the North Atlantic Oscillation on climate through its influence on the Atlantic meridional overturning circulation. *Journal of Climate*, 29(3), 941–962. <https://doi.org/10.1175/JCLI-D-15-0396.1>
- Delworth, T. L., Zeng, F., Vecchi, G. A., Yang, X., Zhang, L., & Zhang, R. (2016). The North Atlantic Oscillation as a driver of rapid climate change in the Northern Hemisphere. *Nature Geoscience*, 9(7), 509–512.
- Dmitrenko, I. A., Polyakov, I. V., Kirillov, S. A., Timokhov, L. A., Frolov, I. E., Sokolov, V. T., et al. (2008). Toward a warmer Arctic Ocean: Spreading of the early 21st century Atlantic Water warm anomaly along the Eurasian Basin margins. *Journal of Geophysical Research*, 113, C05023. <https://doi.org/10.1029/2007JC004158>
- Gent, P. R., Danabasoglu, G., Donner, L. J., Holland, M. M., Hunke, E. C., Jayne, S. R., et al. (2011). The Community Climate System Model Version 4. *Journal of Climate*, 24(19), 4973–4991. <https://doi.org/10.1175/2011JCLI4083.1>
- Gregory, J. M., Dixon, K. W., Stouffer, R. J., Weaver, A. J., Driesschaert, E., Eby, M., et al. (2005). A model intercomparison of changes in the Atlantic thermohaline circulation in response to increasing atmospheric CO₂ concentration. *Geophysical Research Letters*, 32, 112703. <https://doi.org/10.1029/2005GL023209>
- Holland, M., & Bitz, C. (2003). Polar amplification of climate change in coupled models. *Climate Dynamics*, 21, 221–232.
- Huber, M. B., & Zanna, L. (2017). Drivers of uncertainty in simulated ocean circulation and heat uptake. *Geophysical Research Letters*, 44, 1402–1413. <https://doi.org/10.1002/2016GL071587>
- Hwang, Y.-T., Frierson, D. M. W., & Kay, J. E. (2011). Coupling between Arctic feedbacks and changes in poleward energy transport. *Geophysical Research Letters*, 38, 117704. <https://doi.org/10.1029/2011GL048546>
- Jungclaus, J. H., Lohmann, K., & Zanchettin, D. (2014). Enhanced 20th-century heat transfer to the Arctic simulated in the context of climate variations over the last millennium. *Climate of the Past*, 10(6), 2201–2213. <https://doi.org/10.5194/cp-10-2201-2014>
- Koenig, T., & Brodeau, L. (2014). Ocean heat transport into the Arctic in the twentieth and twenty-first century in EC-Earth. *Climate Dynamics*, 42(11), 3101–3120. <https://doi.org/10.1007/s00382-013-1821-x>
- Kostov, Y., Armour, K. C., & Marshall, J. (2014). Impact of the Atlantic meridional overturning circulation on ocean heat storage and transient climate change. *Geophysical Research Letters*, 41, 2108–2116. <https://doi.org/10.1002/2013GL058998>
- Li, D., Zhang, R., & Knutson, T. (2017). On the discrepancy between observed and CMIP5 multi-model simulated Barents Sea winter sea ice decline. *Nature Communications*, 8, 14991.
- Mahajan, S., Zhang, R., & Delworth, T. L. (2011). Impact of the Atlantic meridional overturning circulation (AMOC) on Arctic surface air temperature and sea ice variability. *Journal of Climate*, 24(24), 6573–6581. <https://doi.org/10.1175/2011JCLI4002.1>
- Mahlstein, I., & Knutti, R. (2011). Ocean heat transport as a cause for model uncertainty in projected Arctic warming. *Journal of Climate*, 24(5), 1451–1460. <https://doi.org/10.1175/2010JCLI3713.1>
- Marshall, J., Armour, K. C., Scott, J. R., Kostov, Y., Hausmann, U., Ferreira, D., et al. (2015). The ocean's role in polar climate change: Asymmetric Arctic and Antarctic responses to greenhouse gas and ozone forcing. *Philosophical Transactions of the Royal Society*, 372, 20130040.
- Marshall, J., Scott, J. R., Armour, K. C., Campin, J.-M., Kelley, M., & Romanou, A. (2014). The ocean's role in the transient response of climate to abrupt greenhouse gas forcing. *Climate Dynamics*, 44(7), 2287–2299. <https://doi.org/10.1007/s00382-014-2308-0>
- Menary, M. B., Hodson, D. L. R., Robson, J. I., Sutton, R. T., Wood, R. A., & Hunt, J. A. (2015). Exploring the impact of CMIP5 model biases on the simulation of North Atlantic decadal variability. *Geophysical Research Letters*, 42, 5926–5934. <https://doi.org/10.1002/2015GL064360>
- Nummelin, A., Li, C., & Hezel, P. J. (2017). Connecting ocean heat transport changes from the midlatitudes to the Arctic ocean. *Geophysical Research Letters*, 44, 1899–1908. <https://doi.org/10.1002/2016GL071333>
- Piecuch, C. G., & Ponte, R. M. (2011). Importance of circulation changes to atlantic heat storage rates on seasonal and interannual time scales. *Journal of Climate*, 25, 350–362. <https://doi.org/10.1175/JCLI-D-11-00123.1>
- Pithan, F., & Mauritsen, T. (2014). Arctic amplification dominated by temperature feedbacks in contemporary climate models. *Nature Geoscience*, 7(3), 181–184. <https://doi.org/10.1038/ngeo2071>
- Rugenstein, M. A. A., Winton, M., Stouffer, R. J., Griffies, S. M., & Hallberg, R. (2013). Northern high-latitude heat budget decomposition and transient warming. *Journal of Climate*, 26(2), 609–621. <https://doi.org/10.1175/JCLI-D-11-00695.1>
- Schauer, U., Fahrbach, E., Osterhus, S., & Rohardt, G. (2004). Arctic warming through the Fram Strait: Oceanic heat transport from three years of measurements. *Journal of Geophysical Research*, 109, C06026. <https://doi.org/10.1029/2003JC001823>
- Serreze, M. C., Barrett, A. P., Stroeve, J. C., Kindig, D. N., & Holland, M. M. (2009). The emergence of surface-based Arctic amplification. *The Cryosphere*, 3(1), 11–19. <https://doi.org/10.5194/tc-3-11-2009>
- Singh, H. A., Rasch, P. J., & Rose, B. E. J. (2017). Increased ocean heat transport convergence into the high latitudes with CO₂ doubling enhances polar-amplified warming. *Geophysical Research Letters*, 44, 10583–10591. <https://doi.org/10.1002/2017GL074561>
- Skagseth, Ø., Furevik, T., Ingvaldsen, R., Loeng, H., Mork, K. A., Orvik, K. A., & Ozhigin, V. (2008). *Volume and heat transports to the Arctic Ocean via the Norwegian and Barents Seas* (pp. 45–64). Netherlands, Dordrecht: Springer. https://doi.org/10.1007/978-1-4020-6774-7_3
- Smeed, D. A., McCarthy, G. D., Cunningham, S. A., Frajka-Williams, E., Rayner, D., Johns, W. E., et al. (2014). Observed decline of the Atlantic meridional overturning circulation 2004–2012. *Ocean Science*, 10(1), 29–38. <https://doi.org/10.5194/os-10-29-2014>
- Taylor, K. E., Stouffer, R. J., & Meehl, G. A. (2012). An overview of CMIP5 and the experiment design. *Bulletin of the American Meteorological Society*, 93(4), 485–498. <https://doi.org/10.1175/BAMS-D-11-00094.1>
- Thornalley, D. J. R., Oppo, D. W., Ortega, P., Robson, J. I., Brierley, C. M., Davis, R., et al. (2018). Anomalously weak Labrador Sea convection and Atlantic overturning during the past 150 years. *Nature*, 556(7700), 227–230. <https://doi.org/10.1038/s41586-018-0007-4>
- Yeager, S. (2015). Topographic coupling of the Atlantic overturning and gyre circulations. *Journal of Physical Oceanography*, 45(5), 1258–1284. <https://doi.org/10.1175/JPO-D-14-0100.1>
- Yeager, S. G., Karspeck, A. R., & Danabasoglu, G. (2015). Predicted slowdown in the rate of Atlantic sea ice loss. *Geophysical Research Letters*, 42, 10,704–10,713. <https://doi.org/10.1002/2015GL065364>
- Zhang, R. (2015). Mechanisms for low-frequency variability of summer Arctic sea ice extent. *Proceedings of the National Academy of Sciences*, 112(15), 4570–4575. <https://doi.org/10.1073/pnas.1422296112>